IOSR Journal of Applied Chemistry (IOSR-JAC)
e-ISSN: 2278-5736.Volume 16, Issue 10 Ser. I (October 2023), PP 19-31
www.iosrjournals.org

Enhancement Of The Biological Activity For Esterified Polyethylene Glycols By Blending Them With Sr –Co Nanoferrites

Ahmed I. Adawy[1], Amina I. Ghoneim[2] , Zizi I. Abdeen[1]
[1](Petrochemicals Department, Egyptian Petroleum Research Institute (EPRI) Cairo, Egypt)
[2](Faculty Of Science, Tanta University, Tanta, Egypt)

Abstract
The poly (ethylene glycols) (PEG) was esterified with lauric acid or myristic acid, and their biological activities were improved by blending them with $Sr_{0.25}Co_{0.75}Fe_2O_4$ nanoparticles. The $Sr_{0.25}Co_{0.75}Fe_2O_4$ nanoparticles were prepared by the chemical co-precipitation method. These prepared polymeric surfactants were investigated using Fourier transform infrared spectroscopy (FT-IR), Transmission Electron Microscope (TEM) and diffraction of X-ray (XRD). Also, the surface tension was characterized at diverse temperatures for these compounds. In addition, the surface parameters as well as concentration of critical micelle (CMC), excess of maximum surface (Γ_{max}), area of minimum surface (A_{min}), efficiency (Pc_{20}) and effectiveness (π_{CMC}) were measured and computed. It was assessed and assigned the biological activity of these designed surfactants through length of the field of the hindrance against different microorganisms. It was found as of the results, that these compounds have good surface properties and good biological activity by blending these prepared polymeric surfactants with $Sr_{0.25}Co_{0.75}Fe_2O_4$ to obtain polymeric surfactants nanocomposites for enhancing their biological activity.

Keywords: *Esterification; Biological Activities; Surface properties; $Sr_{0.25}Co_{0.75}Fe_2O_4$ nanoparticles*

Date of Submission: 06-10-2023 Date of Acceptance: 16-10-2023

I. INTRODUCTION

Many applications in industry are found for nonionic surfactants those are cheaply produced, e.g., inhibitors of corrosion, biocides, cosmetics and detergents. Particularly, surfactants could be used as bactericidal agents owing to their nature of amphiphilic and affinity to act together with biological membranes according to Vaara[1] and Schreier et al.[2]. The surface activity of these nonionic surfactants is enhanced by mixing them with cationic or anionic surfactants. Although, the polyethoxylated products are predominated in the marketplace, that are a polyethylene glycol [3,4,5]chain with hydrophilic groups produced by the polycondensation of ethylene oxide on a amino or hydroxyl group. Where, the industrial applicability of nonionic surfactants[5] is enhanced by the existence of a chain of polyoxyethylene. The surfactants applications have unlimited to the nanotechnology field and the cohabitation of nanoparticles and surfactants be able to cause combined effects on biological systems and the environment. The earlier studies have revealed that the nanoparticles mixtures and surfactants showed evidence of effects on organisms by two different joint: (1) surfactants be able to join to the nanoparticles surface, which modify the nanoparticles surface charge and so their toxicity and dispersibility[6] and (2) surfactants that adsorbed on the nanoparticles surface be able to restrain the interaction between nanoparticles and bacteria throughout steric hindrance and charge repulsion and therefore diminish the nanoparticles toxicitie[7]. The combining of nanoparticles and surfactants at the interface is the significant area of research particularly in their application to enhance the constancy of foams and emulsions[8,9]. Ferrite nanoparticles[10] present probable applications in diversity of biomedical fields such as magnetically guided drug delivery, magnetic hyperthermia and magnetic resonance imaging[11,12]. These applications are depending on the ferrite properties that consecutively are inclined by preparation circumstances, such as, size and shape of the nanoparticles. As a result, stand on the application a suitable synthesis method have to be elected to attain definite efficiency. The magnetic nanoparticles application like antimicrobial agents is ahead significance because of the actuality that they be capable of easily control by an outside magnetic field. The required peculiar features claimed for biomedical utilizations of ferri-magnetic nanocrystals are delicate adjustment of nanoparticle's size, antimicrobial merits, and bio-compatibility[13]. Regarding geometrical cationic disposition of Cobalt Nano-spinels ($CoFe_2O_4$) nanocrystals, thus, they possess an inverse Nano-spinel structure with synchronized ferromagnetic merits that protrude from the existence of anti-parallel spins between $Fe^{3+}$and Sr^{2+}cations at tetrahedral A-sites and Co^{2+}cations at octahedral B-sites. Recipro cation of Co^{2+}cations in Nano-

spinels with other alternative transition cations or divalent cations procure enormous discriminatory traits, which are susceptive for amendment to be utilized in assorted skylines. Assorted inspection collections have scrutinized the leverage of commutation with varied cationic sorts to ameliorate the physical traits of Nano-spinels[14]. In our work, nanostructure of non-ionic surfactants were prepared by esterified of poly (ethylene glycol) (PEG) with lauric acid or myristic acid and the biological activities of them were improved by blending them with $Sr_{0.25}Co_{0.75}Fe_2O_4$ nanoparticles. These nanostructure compounds were characterized by investigating their surface activities and structures. As well, the technique of the inhibition zone diameter against diverse microorganisms is used to evaluate and determine their biological activity.

II. MATERIAL AND METHODS

Preparation of $Sr_{0.25}Co_{0.75}Fe_2O_4$ nanoparticles

Nano-spinel $Sr_{0.25}Co_{0.75}Fe_2O_4$crystals was contrived by the explicit co-precipitation methodology utilizing the expression[15,16].

$$0.25\ Sr(NO_3)_2 + 0.75\ Co(NO_3).6H_2O + 2Fe(NO_3)_3.9H_2O + 8(NaOH) \rightarrow Sr_{0.25}Co_{0.75}Fe_2O_4 + 8NaNO_3 + 26.5\ H_2O$$

Delicate proportions of $Sr(NO_3)_2$,$Co(NO_3).6H_2O$, and $Fe(NO_3)_3.9H_2O$ were immersed and stirred in distilled water and reserved at 10ºC for 1 hr. Metal nitrates were continually stirred utilizing a magnetic stirrer, rising pH-reading of stirred sol. by persistent adjustment using NaOH sol. drop-by-drop until PH approach 12. Thereafter, sol. was heated approaching 80 ºC for 2 hrs over continued stirring. Nano-precipitates were extensively bathed with distilled H_2O awaiting Nano-precipitates disposal of $NaNO_3$. Then, Nano-precipitates were dried for a couple of days at room temperature. Afterwards, Nano-precipitates were extensively ground in a detergent agate mortar to acquire ultra-fine powders[15,16].

Synthesis of the Polyethylene glycol esters

0.1 mole of polyethylene glycol, Mw =600 and equal moles of fatty acids (lauric acid and myristic acid) were reacted in xylene (150 mL). A 0.01% p-toluene sulphonic acid like a catalyst (dehydrating agent) was added to the reaction vessel. The reaction was proceeded under heating state (140 ºC) to obtain 1.8 mL of expected water that collected in Dean-Stark equipment. Finally, the solvent was vaporized under lower pressure at 70 ºC. The formed non-ionic surfactants were marked as (Ia) and (IIa), for laurate and myristate correspondingly, Scheme (1).

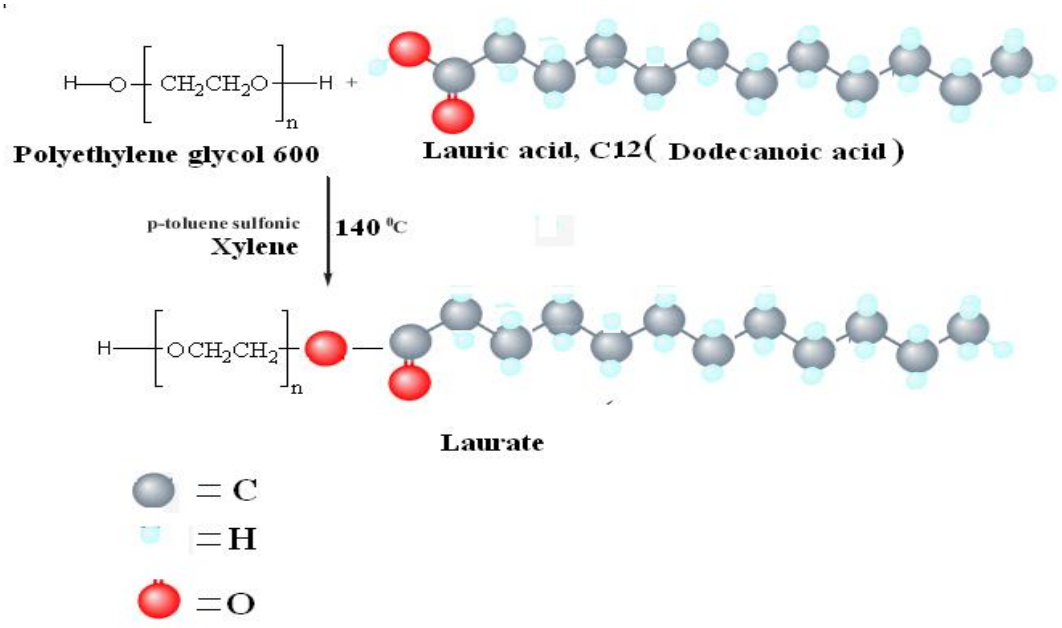

Ia

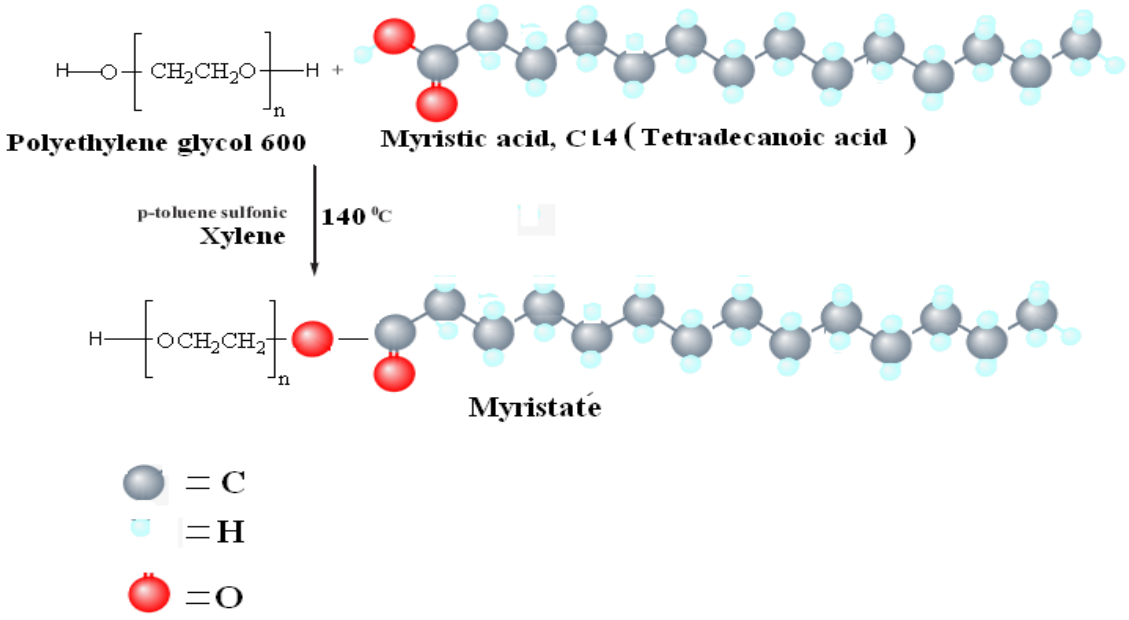

IIa

Scheme (1): Non ionic laurate polyethylene glycol (Ia) and myristate polyethylene glycol (IIa), n = Ethylene glycol repeated units (M.wt=600).

Synthesis of the nanostructure of non-ionic surfactants with $Sr_{0.25}Co_{0.75}Fe_2O_4$ nanoparticles

The nanoparticles solution (20 mL) was blended with 5 mL solution of the prepared nonionic surfactants (Ia, IIa) (0.01 mol) in distilled water. The blend was stirred continually for a day until the color alters to form surfactant nanostructures Ib and IIb [17].

Spectral measurements

Nano-spinel $Sr_{0.25}Co_{0.75}Fe_2O_4$particles were characterized by XRD plots utilizing GNR APD 2000 Pro X-ray diffractometer step-scan type and $CuK_{\alpha 1}$ radiation with wavelength $\lambda = 1.540598$Å.

Lattice parameter *a* for Nano-spinelcrystals was elicited utilizing the expression[18]; $a = d_{hkl}(h^2+k^2+l^2)^{1/2}$

, where (hkl) are miller indices and d_{hkl} is the inter-planer distance given by Bragg's expression[18]: $n\lambda = 2 d_{hkl} \sin\theta$

, reflection order n = 1, θ is Bragg's angle.

Theoretical density D_x (X-ray density) was computed from the relation [19]: $D_x = \frac{ZM}{N_A V} gmcm^{-3}$

, molecular weight is M, Avogadro's number $N_A = 6.023*10^{23}$ molecular/mole, molecules no. per unit cell Z = 8 for Nano-spinel structure, and volume of the unit cell is $V = a^3$.

The elicited crystallite size (R) was assigned utilizing the higher intensity diffraction peak (311) and Sherrer's formula[20]: $R = \frac{0.9\lambda}{\beta_{\frac{1}{2}} \cos\theta}$

, where $\beta_{\frac{1}{2}}$ is the full width at half maximum of the peak (311).

Derived unit cell volume V has been contrived from the expression[21]:

$$V (Å^3) = a^3$$

FT-IR spectral inspection for identification of these Nano-spinel $Sr_{0.25}Co_{0.75}Fe_2O_4$ particles was done by using Bruker Tensor 27 FT-IR Spectrometer ranging from 200 to 4000 cm^{-1}, at ambient temperature. Force constant is the second order derivation of the potential energy with respect to the bond length. As the bond length decreases the force constant increases. F_1 and F_2 are the force constant for the A- and B-sites, respectively, and they are depending on each of length of bond and frequency of vibration at these sites.

Force constant F_c elicited utilizing the expression[15,22]:

$$F_c = 4\pi^2C^2\nu^2\mu$$

, where the velocity of light is C , ν is the sub-lattice frequency of vibration and μ is the reduced mass of vibrating atoms, equals about 2.061 x 10^{-23} gm.

Semiconductor Nano-spinel $Sr_{0.25}Co_{0.75}Fe_2O_4$ particles were scrutinized utilizing JEOL JEM–100 SX transmission electron microscope (TEM); after ultra-sonication span of 45 min aiming the delicate separation of such Nano-spinels.

Surface active properties:

Surface tension:

The surface tension of the solutions of the designed polymeric nonionic surfactants and their nanostructures was performed using Du-Nouy Tensiometer (Kruss type 6). The distilled water was utilized for calibrating and for preparation different concentrations from the prepared surfactants and their nanostructures. The surface tension of various concentrations range of 0.04 to 1.9x 10^{-5} mole/liter at varied temperatures (30, 40, 50 and 60 ^oC) was assigned. Each listed surface tension score was the average of three successive estimations.

Surface parameters of the prepared materials:

a) Critical micelle concentration (CMC):

The surface tension technique was used to define the results of the critical micelle concentration of the formed materials. The outcome points of the surface tension were plotted against the related concentrations. The interrupt, alter in the SC curves pointed the CMC.

b) Effectiveness (π_{CMC}):

π_{CMC} is the difference among the surface tension of the pure water (γ_o) and the surface tension of the surfactant solution (γ) at the critical micelle concentration.

$$\pi_{CMC} = \gamma_{o-}\gamma_{CMC} \qquad (1)$$

c) Efficiency (Pc_{20}):

Efficiency (Pc_{20}) is assigned by the concentration (mol/liter) of the surfactant solutions skilled to reduce the surface tension by 20 mN/m.

d) Maximum surface excess Γ_{max}:

The data of the maximum surface excess Γ_{max} computed from the surface or interfacial scores using the Gibbs equation[23]:

$$\Gamma_{max} = - 1 / 2.303\ RT\ (\delta\gamma / \delta \log C)_T \qquad (2)$$

Where

Γ_{max} maximum surface excess in mole/cm^2

R universal gas constant 8.31 x 10^7 ergs $mole^{-1}$ K^{-1}

T absolute temperature (273.2 + ^oC)

$\delta\gamma$ surface pressure in dyne/cm

C surfactant concentration

$(\delta\gamma/ \delta \log C)_T$ is the slope of a plot surface tension vs. –log concentration curves below CMC at constant temperature.

e) Minimum surface area (A_{min}):

The available space for each molecule at the interface obtains data on the level of loading and the direction of the adsorbed surfactant molecule. The mean area (in square angstrom) settled by every molecule adsorbed on the interface[24] is given by:

$$A_{min} = 10^{16} / \Gamma_{max} N \qquad (3)$$

Γ_{max} maximum surface excess in mole / cm^2

N Avogadro's number 6.023 x 10^{23}

f) Thermodynamic parameters of micellization and adsorption:

The thermodynamic parameters of adsorption and micellization of the designed nonionic surfactants were computed utilizing the Gibb's adsorption equations number (4) as follows[25]:

$$\Delta G^O_{mic} = RT \ln (CMC)$$
$$\Delta G^O_{ads} = \Delta G^O_{mic} - 6.023\ X10^{-1}\ X\ \pi_{CMC}\ X\ A_{min}$$
$$\Delta S_{mic} = - d\ (\Delta G^O_{mic} / \Delta T) \qquad (4)$$
$$\Delta S_{ads} = - d\ (\Delta G^O_{ads} / \Delta T)$$
$$\Delta H_{mic} = \Delta G^O_{mic} + T\ \Delta S_{mic}$$
$$\Delta H_{ads} = \Delta G^O_{ads} + T\ \Delta S_{ads}$$

The activity of the synthesized compounds as antimicrobial:

The activity of the prepared nonionic surfactants as antimicrobial was elected separately in opposition to a significant series of microorganisms previous isolated in Biotechnology Lab. in Egyptian Petroleum Research Institute (EPRI) from a variety of contaminated environments with petroleum using dose equal to 2 mg/ml by using technique of the diffusion agar. The investigated materials were predictable against Gram -ve bacteria (Escherichia coli and Pseud. aeruginosa), Gram +ve bacteria (Bacillus subtilis and Staph. aureus) and Yeast (Candida albicans) and Filamentous Fungus (Aspergillus niger)[26]. On nutrient agar the bacteria and yeast were cultivated whereas on Czapek`s Dox agar environment, the fungus was cultivated. DMF was used as a negative control exhibited no antimicrobial activity against the screening microorganism and the positive control was Erythromycin for bacteria and Metronidazole for yeast and fungus. In duplicates, all inspections were done and the average of the obtained results is the registered data.

III. RESULTS AND DISCUSSION

Structural Characterizations

FT-IR spectral plots for the as-fabricated Nano-spinel $Sr_{0.25}Co_{0.75}Fe_2O_4$ particles have been registered from 200 to 4000 cm^{-1}, as explained in Fig. 1. Emerged IR vibrational summits are scheduled in Table 1. Six oscillation summits of ν_1, ν_2, ν_4, ν_A, ν_B and ν_T have been protruded in FT-IR spectral diagrams, (Fig. 1). $\nu_1$egressed at 588.22cm^{-1} and $\nu_2$egressed at 389.61cm^{-1}, (table 1), referring towards substantial sprawl vibrations of A-occupational sites ligations; whilst versatile recapture forces for bond-bending vibrations subsist on B-occupational sites[18]. Generally, verification of the evolution of Nano-spinel geometrical structure is affirmed by the entity of both $\nu_1$and ν_2. Similarly, it was explored that ν_4 summit egressed at 246.882 cm^{-1} emphasize the lattice oscillating status of Nano-Spinel geometrical structure and its reliance on divalent cations weights entire A-sites and their ligaments,[15,27] Fe^{2+} - O^{2-} and/or Sr^{2+} - O^{2-} Ternary summit ν_T egressed around ~ 1620.16cm^{-1} in FT-IR spectral diagrams was imputed to retaining H_2O in Nano-spinels[28]. H_2O Nonlinearly abundant molecules have 3- substantial vibrational status: symmetric, asymmetric stretching and scissoring vibration status [28]. In FT-IR spectral plot, the immense and intensive summit around ~ 3423.55 cm^{-1} may be imputed to the stretching vibrational status of H-O-H vibrations as well as to H_2O traces according to Gaba et al. 2018[35]. Vibrational summits ν_A and ν_B were egressed around 846.73 and 1053.106 cm^{-1}. Vibrational summit ν_A, point to the coexistence of Fe^{2+}, Sr^{2+}cations entire the A- sites. Vibrational summit ν_B, point to the coexistence of Fe^{4+}- O^{2-} and Co^{2+} - O^{2-} cations entire B-sites. Protrude of Fe^{4+} cations is imputed to electronical jumping in-between $Fe^{3+}$and bothFe^{2+} and Co^{2+} cations[15].

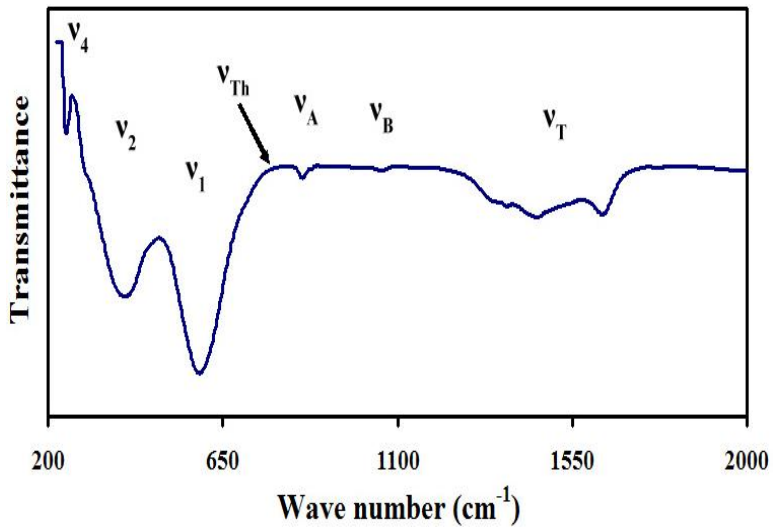

Figure no 1: FT-IR spectral plots of as-prepared $Sr_{0.25}Co_{0.75}Fe_2O_4$ nanocrystals.

Debye temperature was contrived utilizing the expression[29]:

$$\theta_D = \frac{\hbar C \nu_{av}}{k} = 1.438\nu_{av} \text{ and } \nu_{AV} = \frac{\nu_1 + \nu_2}{2}$$

, mean value of wave no's of vibrational summits is ν_{av}, ħ = h/2π, h is the Plank's cons, k is Boltzmann's cons, C = 3×10^{10} cm/s; C is light speed and $\hbar C / k$ = 1.438 for Nano-spinels[29]. Debye temperature θ_D =703.0598 K precisely impressed by IR vibrational summits wave no[29].

Regarding specified thermal energy theorem; evolution of conduction electrons proportion (n-type transporters), substantially procuring some of thermal potency diminishing its saucepan, and this bolsters the conception that conducting status may be assigning to electrons, and vice versa. Threshold frequency ν_{th} egressed at 785.007 cm^{-1} pointing to the transition electrons, thus ν_{th} was acquired from topmost spot of FT-IR spectral diagrams[29]; so that, conduction electron no's possess leverage on ν_{th} and θ_D .

Corresponding threshold energy E_{th} was contrived via the expression[22]:

$$E_{Th} = h \cdot f = h \cdot C \cdot \nu_{Th}$$

, h is Planck's constant, C = 3 × 10^8 m/s is light velocity and ν_{th} is the threshold frequency.

Obviously, the egressed supreme spot ν_{th} protruded at 785.007 cm^{-1} toward higher frequency imputing to the surged hopping process between Fe^{2+} and Fe^{3+}cations. Thence, concluded threshold energy has elevated value as well approaching E_{th} = 0.0973eV,[22]. Otherwise, concluded force constants $F_1$and F_2 for A- and B-occupational allocations orderly equals 2.5337 ×10^5 dyne/cm and 1.11158 ×10^5dyne/cm, affirming reliance of F_1 and F_2 on oscillational frequencies at these allocations, (table 1),[22].

Table no 1: FT-IR vibrational summits positions ν_n; n = 1, 2,…, and B, Threshold frequency ν_{Th}, Debye temperature Θ_D (K), Threshold energy E_{Th}(eV), Force con F_1 and F_2 (dyne/cm), error = ± 0.02.

Nano-Spinel	ν_1 (cm^{-1})	ν_2 (cm^{-1})	ν_4 (cm^{-1})	ν_A (cm^{-1})	ν_B (cm^{-1})	ν_T (cm^{-1})	ν_{Th} (cm^{-1})	Θ_D (K)	E_{Th} (eV)	F_1*10^5 (dyne/m)	F_2*10^5 (dyne/cm)
$Sr_{0.25}Co_{0.75}Fe_2O_4$	588.22	389.61	246.882	846.73	1053.106	1620.16	785.007	703.059	0.0973	2.5337	1.11158

FTIR peaks of each the prepared non ionic laurate polyethylene glycol (Ia) & their nanocomposites (Ib) and myristate polyethylene glycol (IIa), & their nanocomposites (IIb) are similar with a small shift which verify the molecules of the surfactant were accumulated onto the nanoparticles. Fig. 2. was clear that a number of absorption bands such as, The broad bands around 3397 cm^{-1}, is related to the O-H stretching of un-esterified carboxylic acid groups (-COOH) as stated in Kooter et al.[30], whereas those at 2920-2730 cm^{-1} is due to stretching asymmetric and symmetric vibrations of C-H respectively in aliphatic according to Hong et al.[31].

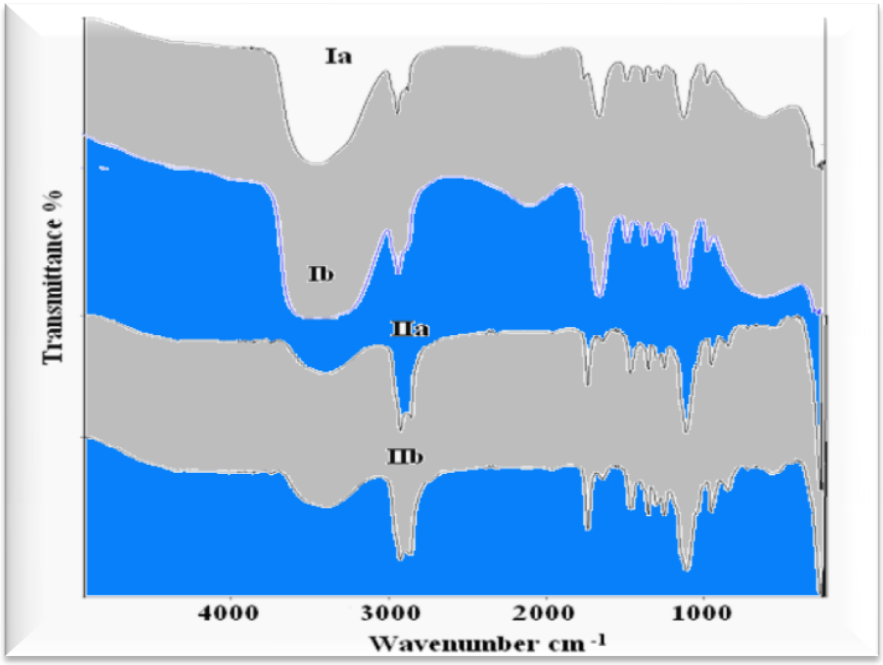

Figure no 2: The FT-IR of Non ionic laurate polyethylene glycol (Ia) & its nanocomposite (Ib) and myristate polyethylene glycol (IIa), & its nanocomposite (IIb) .

The presence of peaks at 2069- 1938 cm^{-1} is related to overtone, whereas the absorption bands at 1627-1536 cm^{-1} are due to C=C, the bending bands of CH_2 around 1457-1456 cm^{-1} and a number of medium bands in the region 1400–1200 cm^{-1} was given to the C-H bending and wagging modes, and O–H bending mode. The peaks with strong intensity at 1088-1038 cm^{-1} were related to the C–O bond stretching mode. The band at 2739

cm^{-1} was endorsed to the C–H aliphatic chain stretching mode of the fatty acids. The extreme IR bands at 1728 cm^{-1} and 1248 cm^{-1} assigned to stretching mode of C=O and C-O respectively, of non ionic laurate polyethylene glycol (Ia) & their nanocomposites (Ib) and myristate polyethylene glycol (IIa), & their nanocomposites (IIb).

Fig.3 explores X-ray diffraction (XRD) plots of the as-synthesized Nano-spinel $Sr_{0.25}Co_{0.75}Fe_2O_4$ particles. Intensively emerging reflection planes affirmed that these Nano-spinels possess one-phase cubic spinel structure[32,33]. Acquired evaluation of the lattice constant a =8.4188 Å matching well with the previous inspections of Nano-spinels[16]. The concluded crystallite size R =10.695 nm, precisely laying in the ultrafine nano-scale and resembling estimations of previously published work[16].

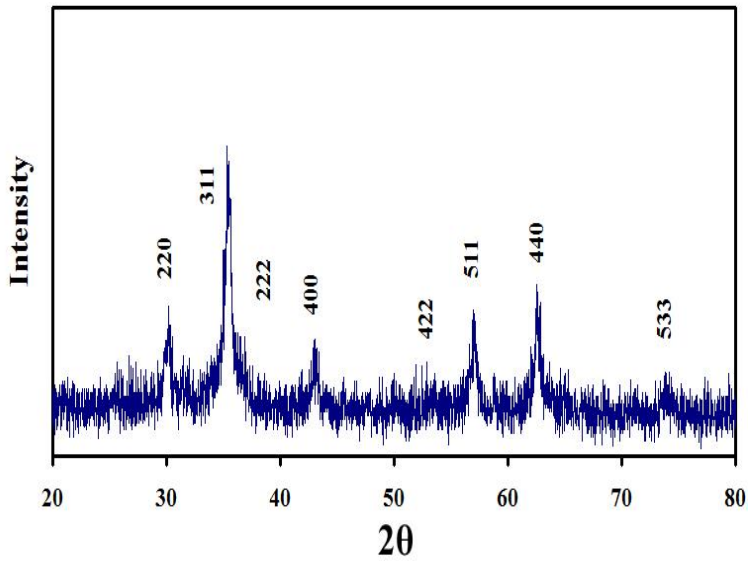

Figure no 3: X-ray diffraction plots for the as-prepared spinel $Sr_{0.25}Co_{0.75}Fe_2O_4$ nanoparticles.

Acquired theoretical X-ray density disclosed a delicate evaluation approaching $D_x \approx 5.3823$ gm/cm^3as seen in Table 2. Whilst, the dimensional unit cell volume provided a precise value approaching V ≈ 596.708 $(Å)^3$, (table 2).

Table no 2: Lattice parameter *a*, the unit cell volume *V*, the crystallite size *R*, the strain *ε,* the X-ray density *Dx*, the specified surface area *S*, the dislocation density δ and the distortion parameter *g*, error = ± 0.02.

Nano-Spinel	*a* (*Å*)	*V* ($Å^3$)	*R* (*nm*)	*E*	D_x (gm/cm^3)	*S* (m^2/gm)	*Δ* $(nm)^{-2}$	*G*
$Sr_{0.25}Co_{0.75}Fe_2O_4$	8.4188	596.708	10.695	-0.0961	5.3823	104.2332	0.00873	0.0427

Dislocation density δ was contrived utilizing the expression[34]:

$$\delta = \frac{1}{R^2}$$, R is the concluded crystallites size.

Distortion parameter g was contrived via the formula[34]:

$$g = \frac{\beta_{1/2}}{\tan\theta}$$

The concluded estimation of the distortion parameter g = 0.0427 and dislocation density δ = 0.00873 nm^{-2}, as seen in table 2. Otherwise, Table 2 discloses reliance of g and δ on R and θ, whilst g and δ rely on interior amendments in Nanocrystal's lattice spacing and oxygen ion concentration[34].

Specified surface area S of Nano-spinels was contrived utilizing[35];

$$S = \frac{6000}{R_{XRD}D_x}$$

Concluded Strain ε for those Nano-spinels was contrived utilizing the derived formula[35];

$$\beta_{1/2}\cos\theta = \frac{0.94\lambda}{R_{XRD}} + 4\varepsilon\sin\theta$$

Ultimately, S provides reliance on both the crystallite size R and X-ray density D_x[36]. On Synchrony, Strain ε = -0.0961 interior these Nano-spinels relies on type of cations and their crystallographic configuration, (table 2), as well as the protruded crystalline anisotropy[37]. Obviously, the ultra-fine size status of these Nano-spinels necessitates that they possess extremely biggest specific surface areas[35].Thence, the specified surface area revealed extremely biggest estimation reaching S ≈ 104.2332 m^2/gm, imputing to ultra-teeny crystallite size R, (table 2). Figure 4 of XRD patterns demonstrating the (Ib) amorphous nature is greater than ever and resulting in decreasing the crystallinity of $Sr_{0.25}Co_{0.75}Fe_2O_4$, wherever the peaks of amorphous diffraction around 2θ =24° are representing the intercalated $Sr_{0.25}Co_{0.75}Fe_2O_4$into the surfactant molecules and demonstrates the successful blending. But, the crystallinity of $Sr_{0.25}Co_{0.75}Fe_2O_4$ slightly decreasing with (IIb) and shift indicating the slightly blending**.**

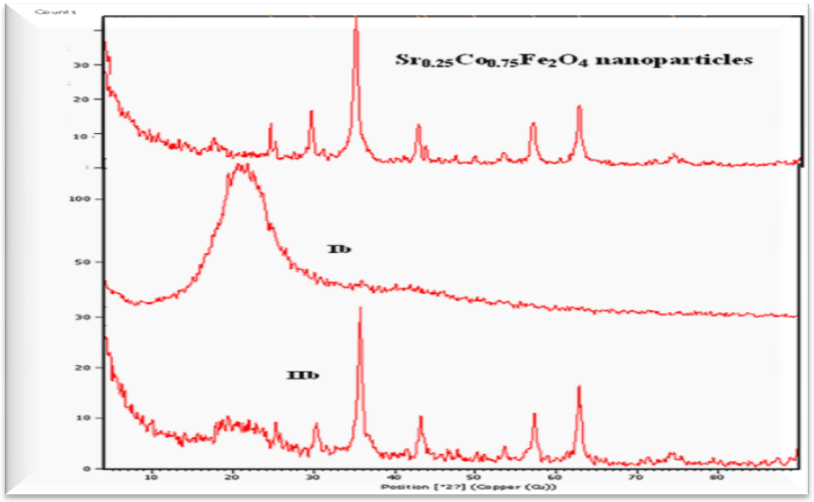

Figure no 4: The XRD patterns of the as-prepared $Sr_{0.25}Co_{0.75}Fe_2O_4$, non ionic laurate polyethylene glycol nanocomposite (Ib) and myristate polyethylene glycol nanocomposite (IIb).

TEM of as-synthesized Nano-spinel $Sr_{0.25}Co_{0.75}Fe_2O_4$ particles are affirmed in Fig.5. Obviously, TEM explores the ultra-teeny nature of these Nano-spinel particles with mean nanoparticle size Z approaching ≈ 11.96 nm. It is explicit that, Z evaluation is closer to that of the crystallite size R, where Z is lightly bigger pointing to the thinning amorphous stratum on superficies of Nano-spinel $Sr_{0.25}Co_{0.75}Fe_2O_4$ particles. This is imputing to the certainty that XRD plots capture only the well-crystalline sector interior Nano-spinel particles, whilst TEM image explore the overall and the complete image of $Sr_{0.25}Co_{0.75}Fe_2O_4$ nanoparticles[33]. TEM image for $Sr_{0.25}Co_{0.75}Fe_2O_4$ Nano-regime clarifies that those nanoparticles are in the Nano-scale and lightly agglomerated and their average particles size Z is precisely approaching ≈ 11.96 nm.

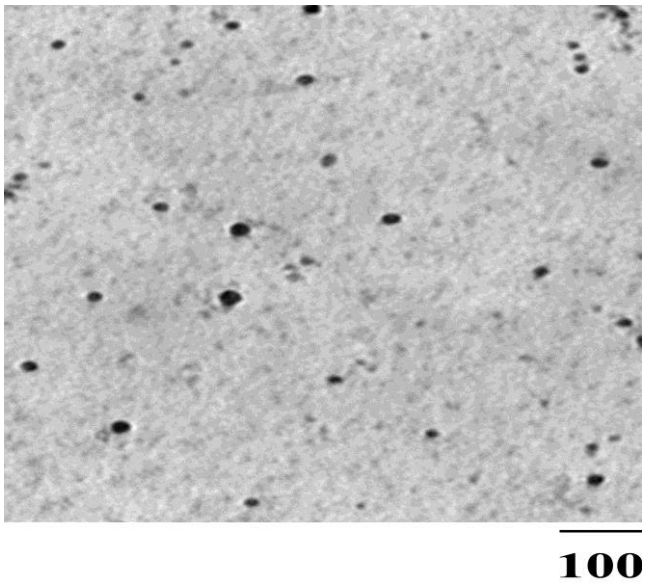

Figure no 5: TEM image of the as-prepared (AP) spinel $Sr_{0.25}Co_{0.75}Fe_2O_4$ nanoparticles.

Surface properties of the prepared metallo-surfactant compounds:

Surface tension

The surface tension was designated for aqueous solutions of the designed nonionic surfactants at various concentrations (0.04 to 1.9X 10^{-5} mole/liter) and at several temperatures 30, 40, 50 and 60 ^{o}C. The information are performed in surface tension-concentration curves as presented in figure (6) and confirmed that the prepared nonionic polymeric surfactants and their nanostructures Ia, IIa, Ib and IIb have good surface activity. The surface tension reduced as the concentration of the surfactants growing due to the presence of the hydrophobic moiety which force excess of surfactants molecules to migrate pointed to the solution surface[38,39]. Moreover, as the result of maximize the temperature from 30 to 60 ^{o}C, the surface tension lowered because of the solubility shortage of surfactants by increasing the temperature due to the hydrophilic moieties were dehydrated to accumulate in the surface[40]. Outcomes of surface tension appeared in Fig (6) exhibits lowering in surface tension scores of the designed surfactants after stabilizing the nanoparticles $Sr_{0.25}Co_{0.75}Fe_2O_4$ against agglomeration more than the singular surfactant which indicates the increase in the solubility of the designed surfactant after assembling on nanoparticles[41] and the nanostructure of the synthesized myristate surfactant (IIb) exhibits the smallest surface tension scores between all the designed compounds.

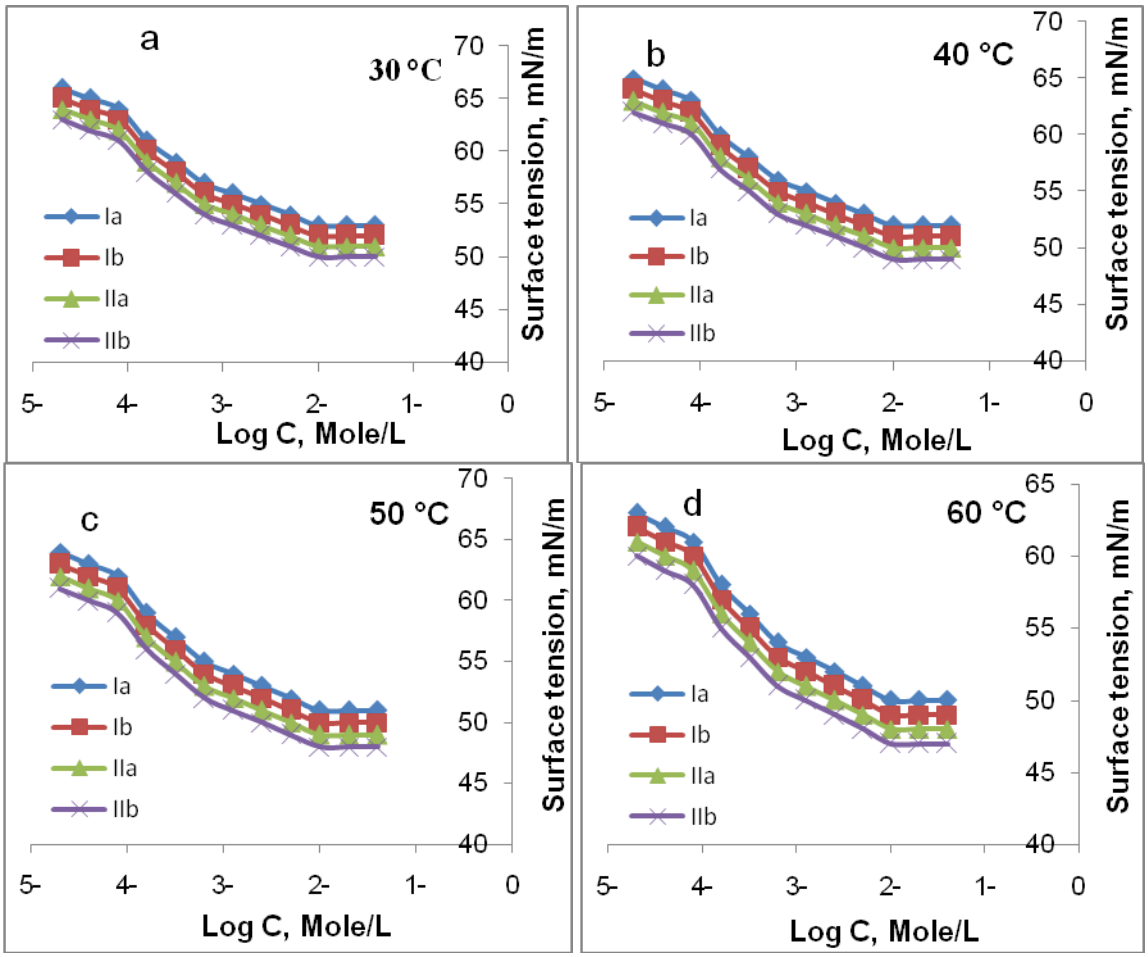

Figure no 6: Surface tension vs. Log Concentration of compounds Ia, IIa and their nanocomposites Ib and IIb at (30, 40, 50 and 60 ^{o}C).

The critical micelle concentration (CMC):

The scores of the critical micelle concentration of the designed nonionic surfactants were assigned by plotting the surface tension (γ) of surfactant solutions against their concentrations in mole/liter at 30, 40, 50 and 60^{o}C. There is a reduce in CMC scores from laurate (Ia) to the nanostructure of the synthesized myristate surfactant (IIb), i.e. as growing of the alky chain length like mentioned in table (3) and this is as a result of increasing the hydrophobicity which obliged the surfactant molecules to collect at the surface and less molecules is required to attain the equilibrium state to form micelles[42]. On the other hand, as the temperature raising the CMC minimize and this is because the lowering in the solvation of the hydrophilic moieties that reinforce the micellization. On the contrary, there is a disarrangement of the regular water molecules border on the

hydrophobic moieties as the temperature increasing that hates micillization[43]. As listed in the table (3) the scores of the CMC reduce with growing the temperature, i.e. an enhancement in the micellization occurred. The values of CMC give also indication about the ability of the prepared surfactant and their nanocomposites to soluble in water. The most minimal CMC scores existed with nanocomposites that indicate the rapid existence of micelles, furthermore the singular surfactants work as capping agents to nanoparticles $Sr_{0.25}Co_{0.75}Fe_2O_4$ the operation that leads to avoid agglomeration of nanoparticles in their solution.

Table no 3: Surface properties of the synthesized compounds at 30, 40, 50, 60 °C.

Surfactant	$CMC\ X\ 10^{-3}$, *Mole/liter*	π_{CMC}, *mN/m*	$Pc_{20}\ X\ 10^{-3}$, *Mole/liter*	$\Gamma_{max}\ X\ 10^{-10}$, *Mole/cm²*	A_{min}, *nm²*
Ia	1.8	16	10	0.9	1.67
Ib	1.6	17	10	1	1.58
IIa 30 °C	1.3	18	5	1.04	1.5
IIb	1.2	19	2.5	1.08	1.5
Ia	1.5	17	7	1	1.63
Ib	1.4	18	5	1.01	1.6
IIa 40 °C	1.2	19	2.5	1	1.58
IIb	1	20	1.2	1.05	1.5
Ia	1.4	18	4	0.9	1.69
Ib	1.1	19	2.5	1	1.63
IIa 50 °C	1	20	1.3	1	1.63
IIb	0.9	21	0.63	1.02	1.6
Ia	1.2	19	2	0.9	1.68
Ib	1	20	1.2	1	1.6
IIa 60 °C	0.9	21	0.63	0.9	1.68
IIb	0.7	22	0.32	1	1.6

Effectiveness (Π_{CMC}):

The most powerful surfactant is that shows the highest lowering in surface tension for a critical micelle concentration (CMC). As listed the scores of the effectiveness in table (3), there is growing in effectiveness of the prepared non ionic surfactants as the alkyl chain length and the temperature maximize as a result of quick existing of micelles. The most potent one is compound (IIb) which has the maximum reduce in surface tension at CMC.

Efficiency (Pc_{20}):

As shown in table (3) the values of efficiency of the prepared surfactants reduce as the hydrophobicity and temperature rising due to quick preparation monolayer of nonionic surfactant on the surface.

Maximum surface excess (Γ_{max}):

As listed in table (3) the scores of Γ_{max} maximize as the hydrophobicity increase due to escaping of surfactant molecules from the bulk of the solution and accumulate in the surface.

Minimum surface area (A_{min}):

As shown in table (3) the values of A_{min} lower with raising the alky chain length of the nonionic surfactants because of reduce the available area per molecule as a result of grouping the surfactant in the surface.

Standard free energies of micellization and adsorption (ΔG^o_{mic}, ΔG^o_{ads}):

The values of ΔG_{mic} and ΔG_{ads} are always negatives as listed in the tables (4,5) indicating of spontaneous operations and the higher scores of ΔG_{ads} comparing to those of micellization referring to trend of surfactant molecules to adsorb in the surface more than formation of micelles.

Table no 4: Thermodynamic parameters of micellization of the synthesized compounds at 30, 40, 50, 60 °C.

Surfactant	ΔG^O_{mic}, *KJ/mole*	ΔH_{mic}, *KJ/mole*
Ia	- 15.9	- 46.2
Ib	- 16.2	- 43.5
IIa 30 °C	- 16.7	- 37.9
IIb	- 16.9	- 47.2
Ia	- 16.9	- 48.2
Ib	- 17.1	- 45.2
IIa 40 °C	- 17.5	- 39.4
IIb	- 17.9	- 49.3
Ia	- 17.6	- 49.9
Ib	- 18.3	- 44.1

IIa 50 °C	- 18.5	- 47.6
IIb	- 18.8	- 60.8
Ia	- 18.6	- 51.9
Ib	- 19.1	- 45.8
IIa 60 °C	- 19.4	- 49.4
IIb	- 20.1	- 63.4

Table no 5: Thermodynamic parameters of adsorption of the synthesized compounds at 30, 40, 50, 60 °C.

Surfactant	ΔG^{O}_{ads}, *KJ/mole*	ΔH_{ads}, *KJ/mole*
Ia	- 32	- 83.5
Ib	- 32.4	- 105.2
IIa 30 °C	- 33.9	- 85.4
IIb	- 34.4	- 113.3
Ia	- 33.7	- 86.9
Ib	- 34.8	- 110
IIa 40 °C	- 35.5	- 88.8
IIb	- 37	- 118.4
Ia	- 35.9	- 97.3
Ib	- 36.9	- 117.7
IIa 50 °C	- 38.2	- 118.9
IIb	- 39.4	- 133.2
Ia	- 37.8	- 101.2
Ib	- 39.4	- 122.7
IIa 60 °C	- 40.7	- 123.9
IIb	- 42.4	- 139

Biological activity of the metallosurfactant compounds:

As a result of being the polar groups in the skeleton of nonionic surfactants, they tend to aggregate in the outside film of the cells causes reduce their osmotic duration driving to die of the microorganism. The biological efficiency of the antimicrobial agents relies on its molecular structure[44]. As outlined in table (6) the prepared polymeric nonionic surfactants and their nanostructures Ia, IIa, Ib and IIb have good biological activity against the tested microorganisms.

The nonionic surfactants are considered one of the powerful biocides as a result of their technique. The oxygen atoms obliged to close the joining region due to its electronegativity. Beside the hydrophobic moieties together with the electrostatic forces, the intrinsic proteins that circle the film of the cell obliged to be grasped in position by the hydrogen bonding. Moreover the hydrogen bonding is arranging disrupt of cell membrane. The hydrophilic zone of the membrane linking to the hydrophilic part of the nonionic surfactant (polyethoxy) via the intermolecular hydrogen bond. In spite of the fact that this is the method of the biocidal potent as a surfactant, the linked zone of the germicidal agent is obscure[45]. Growing the concentration of the biocide leading to more aggregate at varied substrates (aqueous or films of microorganism)[46]. Thus, the more collection of the nonionic surfactants at the film of the cells leading to excess of vigorous act of the molecules toward microorganisms. The inhibition activity of the nanocomposites is higher than that of the individual surfactant. Where, the upgrade in the germicidal potent of the prepared compounds with nanoparticles might be identified with the existence of little-volume nanoparticles in the nanostructure of the C12 and C14 surfactant that getting better the entrance of the surfactant particle to the cell film of the microorganism.

Table no 6: The results of biological activity of the synthesized polymeric surfactants (Ia, IIa) and their nanostructures (Ib, IIb) at 2mg/ml against different microorganisms measured by mm.

Tested organism / Surfactant ID	*Bacillus subtilis* **(Gram+ve)**	*Staph. aureus* **(Gram+ve)**	*Escherichia coli* **(Gram -ve)**	*Pseud. aeruginosa* **(Gram -ve)**	*Candida albicans* **(Yeast)**	*Aspergillus niger* **(Fungi)**
Ia	21	20	19	15	25	15
Ib	20	21	18	20	27	15
IIa	26	28	26	27	30	27
IIb	28	27	28	29	31	33
Reference	**29**	**28**	**28**	**30**	**27**	**30**

IV. CONCLUSION

Two synthesized nonionic polymeric surfactants Ia and IIa based on polyethylene glycol and their nanostructures Ib and IIb were prepared and illustrated their bodies. The surface attitude of the designed

surfactants and their nanostructures in aqueous medium was investigated utilizing surface tension detecting that they have good surface activity and the nanostructure of the synthesized myristate surfactant (IIb), with longer hydrophobic chain length had the lowest critical micelle concentration also the micellization affinity increases with maximize the temperature. Finally, the synthesized nonionic polymeric surfactants gave good biological activity against different microorganisms and blending these prepared polymeric surfactants with $Sr_{0.25}Co_{0.75}Fe_2O_4$ to obtain polymeric surfactants nanocomposites for enhancing their biological activity, where the surface parameters play an important role in their antimicrobial effect.

ACKNOWLEDGMENTS

The authors are appreciative of Egyptian Petroleum Research Institute (EPRI) in parallel with Tanta University for supporting current research

REFERENCES

[1]. Vaara M. Agents That Increase The Permeability Of The Outer Membrane. Microbiol Rev. 1992; 56:395–411. Https://Doi.Org/10.1128/Mr.56.3.395-411.1992
[2]. Schreier S, Malheiros SVP, De Paula E. Surface Active Drugs: Self-Association And Interaction With Membranes And Surfactants. Physicochemical And Biological Aspects. Biochimica Et Biophysica Acta (BBA) – Biomembranes. 2000; 1508:210–234. Https://Doi.Org/10.1016/S0304-4157(00)00012-5
[3]. Abdeen Z. Preparations And Applications Of Some Friendly Environmental Compounds. 2005; Ph.D. Thesis, Ain- Shams University, Cairo, Egypt.
[4]. Abdeen Z. Adsorption Efficiency Of Poly(Ethylene Glycol)/Chitosan/CNT Blends For Maltene Fraction Separation. Environ Sci PollutRes. 2016; 23:11240–11246. Https://Doi.Org/10.1007/S11356-016-6225-0
[5]. Adawy AI, Abdeen ZI, Abdel Rahman NR, Ali HE-S. Evaluation Of The Biological Activity Of The Prepared Nonionic Polymeric Based On The Acrylated Polyethylene Glycol. Journal Of Molecular Liquids. 2019; 288:111010. Https://Doi.Org/10.1016/J.Molliq.2019.111010
[6]. Baalousha M. Aggregation And Disaggregation Of Iron Oxide Nanoparticles: Influence Of Particle Concentration, Ph And Natural Organic Matter. Science Of The Total Environment 2009; 407:2093–2101. Https://Doi.Org/10.1016/J.Scitotenv.2008.11.022
[7]. Zhang LW, Zeng L, Barron AR, Monteiro-Riviere NA. Biological Interactions Of Functionalized Single-Wall Carbon Nanotubes In Human Epidermal Keratinocytes. Int J Toxicol. 2007; 26:103–113. Https://Doi.Org/10.1080/10915810701225133
[8]. Hunter TN, Wanless EJ, Jameson GJ, Pugh RJ. Non-Ionic Surfactant Interactions With Hydrophobic Nanoparticles: Impact On Foam Stability. Colloids And Surfaces A: Physicochemical And Engineering Aspects. 2009; 347:81–89. Https://Doi.Org/10.1016/J.Colsurfa.2008.12.027
[9]. Moghadam TF, Azizian S. Effect Of Zno Nanoparticles On The Interfacial Behavior Of Anionic Surfactant At Liquid/Liquid Interfaces. Colloids And Surfaces A: Physicochemical And Engineering Aspects. 2014; 457:333–339. Https://Doi.Org/10.1016/J.Colsurfa.2014.06.009
[10]. Abdeen ZI, Ghoneim AI. Improving Of The Mg-Co Nanoferrites Efficiency For Crude Oil Adsorption From Aqueous Solution By Blending Them With Chitosan Hydrogel. Environ Sci Pollut Res. 2020; 27:19038–19048. Https://Doi.Org/10.1007/S11356-018-3557-Y
[11]. Sheena Xavier, Harry Cleetus, Nimila PJ., Smitha Thankachan, Rintu Mary Sebastian, Mohammed EM., Synthesis, Characterization And Antibacterial Activity Of Silver Substituted Cobalt Ferrite Nanoparticles, Research Journal Of Pharmaceutical, Biological And Chemical Sciences, Accepted.
[12]. Xavier S, Jiji MK, Thankachan S, Mohammed EM. Effect Of Sintering Temperature On The Structural And Electrical Properties Of Cobalt Ferrite Nanoparticles. Kochi, Kerala, India. 2014;98–101
[13]. Hashim Mohd, Alimuddin, Shirsath SE, Et Al. Investigation Of Structural, Dielectric, Magnetic And Antibacterial Activity Of Cu–Cd–Ni– Feo4 Nanoparticles. Journal Of Magnetism And Magnetic Materials. 2013; 341:148–157. Https://Doi.Org/10.1016/J.Jmmm.2013.04.024
[14]. Goldman A. Modern Ferrite Technology, 2nd Ed. Springer. 2005; New York, NY
[15]. Amer MA, Meaz TM, Attalah SS, Ghoneim AI. Structural And Magnetic Characterization Of The Mg0.2−Xsrxmn0.8Fe2O4 Nanoparticles. Journal Of Magnetism And Magnetic Materials. 2014; 363:60–65. Https://Doi.Org/10.1016/J.Jmmm.2014.03.067
[16]. Hankare PP, Vader VT, Patil NM, Et Al. Synthesis, Characterization And Studies On Magnetic And Electrical Properties Of Mg Ferrite With Cr Substitution. Materials Chemistry And Physics. 2009; 113:233–238. Https://Doi.Org/10.1016/J.Matchemphys.2008.07.066
[17]. Negm NA, Tawfik SM, Abd-Elaal AA. Synthesis, Characterization And Biological Activity Of Colloidal Silver Nanoparticles Stabilized By Gemini Anionic Surfactants. Journal Of Industrial And Engineering Chemistry. 2015; 21:1051–1057. Https://Doi.Org/10.1016/J.Jiec.2014.05.015
[18]. Cullity BD, Cullity BD. Introduction To Magnetic Materials. Addison-Wesley, 1972; Reading, Mass.
[19]. Safaan SA, Abo El Ata AM, El Messeery MS. Study Of Some Structural And Magnetic Properties Of Mn-Substituted Srcu Hexagonal Ferrites. Journal Of Magnetism And Magnetic Materials. 2006; 302:362–367. Https://Doi.Org/10.1016/J.Jmmm.2005.09.041
[20]. Cullity BD. Elements Of X-Ray Diffraction, 2d Ed. Addison-Wesley Pub. Co. 1978; Reading, Mass
[21]. Yadav RS, Havlica J, Masilko J, Et Al. Impact Of Nd3+ In Cofe2o4 Spinel Ferrite Nanoparticles On Cation Distribution, Structural And Magnetic Properties. Journal Of Magnetism And Magnetic Materials. 2016; 399:109–117. Https://Doi.Org/10.1016/J.Jmmm.2015.09.055
[22]. Modi KB, Shah SJ, Pujara NB, Et Al. Infrared Spectral Evolution, Elastic, Optical And Thermodynamic Properties Study On Mechanically Milled Ni0.5Zn0.5Fe2O4 Spinel Ferrite. Journal Of Molecular Structure. 2013; 1049:250–262. Https://Doi.Org/10.1016/J.Molstruc.2013.06.051
[23]. Zhou M, Luo G, Zhang Z, Et Al. Synthesis And Properties Evaluation Of Sulfobetaine Surfactant With Double Hydroxyl. Journal Of Molecular Structure. 2017: 1144:199–205. Https://Doi.Org/10.1016/J.Molstruc.2017.05.023
[24]. Shuichi, M, Kazayasu I, Sadao Y, Kazuo K,Tsuyoshi Y. Surface Activities, Biodegradability And Antimicrobial Properties Of N-Alkyl Glucosides, Mannosides And Galactosides, J. Am. Oil Chem. Soc. 1991; 67 (12) :996 – 1001; Https://Doi.Org/ 10.1007 /BF02541865

[25]. Rosen MJ. Surfactants And Interfacial Phenomena. John Wiley & Sons, Inc. 2004; Hoboken, NJ, USA
[26]. Shaban SM, Aiad I, Moustafa AH, Aljoboury OH. Some Alginates Polymeric Cationic Surfactants; Surface Study And Their Evaluation As Biocide And Corrosion Inhibitors. Journal Of Molecular Liquids. 2019; 273:164–176. Https://Doi.Org/10.1016/J.Molliq.2018.10.017
[27]. Hashim Mohd, Alimuddin, Kumar S, Et Al (2012) Structural Properties And Magnetic Interactions In Ni0.5Mg0.5Fe2−Xcrxo4 ($0 \leq X \leq 1$) Ferrite Nanoparticles. Powder Technology 229:37–44. Https://Doi.Org/10.1016/J.Powtec.2012.05.054
[28]. Saafan SA, Meaz TM, El-Ghazzawy EH, Et Al. A.C. And D.C. Conductivity Of Nizn Ferrite Nanoparticles In Wet And Dry Conditions. Journal Of Magnetism And Magnetic Materials 2010 ; 322:2369–2374. Https://Doi.Org/10.1016/J.Jmmm.2010.02.039
[29]. Patange SM, Shirsath SE, Lohar KS, Et Al. Infrared Spectral And Elastic Moduli Study Of Nife2−Xcrxo4 Nanocrystalline Ferrites. Journal Of Magnetism And Magnetic Materials 2013; 325:107–111. Https://Doi.Org/10.1016/J.Jmmm.2012.08.022
[30]. Kooter IM, Pierik AJ, Merkx M, Et Al. Difference Fourier Transform Infrared Evidence For Ester Bonds Linking The Heme Group In Myeloperoxidase, Lactoperoxidase, And Eosinophil Peroxidase. J Am Chem Soc. 1997; 119:11542–11543. Https://Doi.Org/10.1021/Ja9725460
[31]. Hong R-Y, Li J-H, Zhang S-Z, Et Al. Preparation And Characterization Of Silica-Coated Fe3O4 Nanoparticles Used As Precursor Of Ferrofluids. Applied Surface Science. 2009; 255:3485–3492. Https://Doi.Org/10.1016/J.Apsusc.2008.09.071
[32]. Verma K, Kumar A, Varshney D. Dielectric Relaxation Behavior Of Axco1−Xfe2o4 (A=Zn, Mg) Mixed Ferrites. Journal Of Alloys And Compounds. 2012; 526:91–97. Https://Doi.Org/10.1016/J.Jallcom.2012.02.089
[33]. Phumying S, Labuayai S, Swatsitang E, Et Al. Nanocrystalline Spinel Ferrite (Mfe2o4, M=Ni, Co, Mn, Mg, Zn) Powders Prepared By A Simple Aloe Vera Plant-Extracted Solution Hydrothermal Route. Materials Research Bulletin. 2013; 48:2060–2065. Https://Doi.Org/10.1016/J.Materresbull.2013.02.042
[34]. Kumar V, Ali Y, Sonkawade RG, Dhaliwal AS. Effect Of Gamma Irradiation On The Properties Of Plastic Bottle Sheet. Nuclear Instruments And Methods In Physics Research Section B: Beam Interactions With Materials And Atoms. 2012; 287:10–14. Https://Doi.Org/10.1016/J.Nimb.2012.07.007
[35]. Dixit G, Pal Singh J, Srivastava RC, Agrawal HM. Magnetic Resonance Study Of Ce And Gd Doped Nife2o4 Nanoparticles. Journal Of Magnetism And Magnetic Materials. 2012; 324:479–483. Https://Doi.Org/10.1016/J.Jmmm.2011.08.027
[36]. Amer MA, Meaz TM, Hashhash A, Et Al. Structural Properties And Magnetic Interactions In Sr-Doped Mg–Mn Nanoparticle Ferrites. Materials Chemistry And Physics. 2015; 162:442–451. Https://Doi.Org/10.1016/J.Matchemphys.2015.06.013
[37]. Lenin N, Rajesh Kanna R, Sakthipandi K, Senthil Kumar A. Structural, Electrical And Magnetic Properties Of Nila Fe2-O4 Nanoferrites. Materials Chemistry And Physics 2018; 212:385–393. Https://Doi.Org/10.1016/J.Matchemphys.2018.03.062
[38]. Perinelli DR, Petrelli D, Vitali LA, Et Al. Quaternary Ammonium Surfactants Derived From Leucine And Methionine: Novel Challenging Surface Active Molecules With Antimicrobial Activity. Journal Of Molecular Liquids. 2019; 283:249–256. Https://Doi.Org/10.1016/J.Molliq.2019.03.083
[39]. Aiad I, Abo Riya M, Tawfik SM, Abousehly MA. Synthesis, Surface Properties And Biological Activity Of N,N,N-Tris(Hydroxymethyl)-2-Oxo-2-(2-(2-(Alkanoyloxy) Ethoxy)Ethoxy) Ethanaminium Chloride Surfactants. Egyptian Journal Of Petroleum 2016; 25:299–307. Https://Doi.Org/10.1016/J.Ejpe.2015.07.020
[40]. Adawy AI, Khowdiary MM. Structure And Biological Behaviors Of Some Metallo Cationic Surfactants. Journal Of Surfactants And Detergents. 2013;16:709–715. Https://Doi.Org/10.1007/S11743-013-1483-Z
[41]. Azzam EMS, Zaki MF. Surface And Antibacterial Activity Of Synthesized Nonionic Surfactant Assembled On Metal Nanoparticles. Egyptian Journal Of Petroleum. 2016; 25:153–159. Https://Doi.Org/10.1016/J.Ejpe.2015.04.005
[42]. Negm NA, El Hashash MA, Youssif MA, Et Al. Novel Nonionic Polyurethane Surfactants And Ag Nanohybrids: Influence Of Nonionic Polymeric Chains. J Surfact Deterg. 2017; 20:173–182. Https://Doi.Org/10.1007/S11743-016-1909-5
[43]. Adawy AI. Preparation And Evaluation Of Some Amide Based Cationic Surfactants As Biocides, J. Surface Sci. Technol. 2017; 33(3–4):83–90; Https://Doi.Org/ 10.18311 /Jsst/2017/15653.
[44]. El-Sukkary MMA, Shaker NO, Ismail DA, Et Al. Surface Parameters, Biodegradability And Antimicrobial Activity Of Some Amide Ether Carboxylates Surfactants. Egyptian Journal Of Petroleum. 2012; 21:37–43. Https://Doi.Org/10.1016/J.Ejpe.2012.02.006
[45]. Tawfik SM, Zaky MF, Mohammad TGM, Attia HAE. Synthesis, Characterization, And In Vitro Antifungal Activity Of Anionic And Nonionic Surfactants Against Crop Pathogenic Fungi. Journal Of Industrial And Engineering Chemistry. 2015; 29:163–171. Https://Doi.Org/10.1016/J.Jiec.2015.03.031
[46]. Adawy AI, Abbas MA, Zakaria K. Synthesis, Characterization, And Surface Activity Of Some Schiff Base Cationic Surfactant Complexes Against Different Microorganisms. Petroleum Science And Technology. 2015; 33:1348–1356. Https://Doi.Org/10.1080/10916466.2015.1060500